Journal of Photochemistry and Photobiology A: Chemistry 217 (2011) 236–241

Contents lists available at ScienceDirect

Journal of Photochemistry and Photobiology A: Chemistry

journal homepage: www.elsevier.com/locate/jphotochem

Electron dynamics dependence on optimum dye loading for an efficient dye-sensitized solar cell

G. Kantonis [a], T. Stergiopoulos [a,*], A.P. Katsoulidis [b], P.J. Pomonis [b], P. Falaras [a,*]

[a] Institute of Physical Chemistry, NSCR "Demokritos", 15310 Aghia Paraskevi Attikis, Athens, Greece
[b] Department of Chemistry, University of Ioannina, 45 444 Ioannina, Greece

ARTICLE INFO

Article history:
Received 18 August 2010
Received in revised form
29 September 2010
Accepted 14 October 2010
Available online 23 October 2010

Keywords:
Titania annealing
Electron transport
Recombination
Dye loading
Dye-sensitized solar cells

ABSTRACT

Increasing surface area and optimum dye loading are among the prerequisites for an efficient TiO_2-based dye-sensitized solar cell (DSC), since they improve light harvesting but, at the same time, affect, in a variant way the electron dynamics in the semiconductor. Into this context, in this work, the interdependence of these two effects was investigated. The thermal annealing conditions of nanocrystalline titania films were modified between 400 and 550 °C in order to vary the crystallinity and the aggregation/sintering degree of the semiconductor particles. The annealing effects on the structural and surface parameters of the films were determined and the electron dynamics inside the semiconductor were elucidated. The film properties were found to correlate with the photoelectric conversion efficiencies of the corresponding DSCs in terms of light harvesting efficiency, electron transport, recombination and trapping at surface states. Despite higher dye loading, a relatively low efficiency (5.3%) was attained at the temperature of 400 °C, due to insufficient neck growth and the presence of surface states that were not removed by annealing. On the contrary, the highest efficiency (6.4%) was attained at 550 °C, where high values of electron diffusion coefficients and enhanced electron lifetimes were observed despite a significantly lower dye loading. The above results point out the significance of properly controlling both light harvesting and electron dynamics in the photoelectrode for efficient dye sensitization of a large band gap semiconductor.

1. Introduction

Dye solar cells (DSCs) are intensely investigated as the main representatives of third generation photovoltaics [1]. This type of photovoltaic device consists of three main parts: the semiconductor (a nanostructured film of TiO_2 deposited on conductive substrate), the dye (a Ru(II) metallorganic complex endowed with polypyridyl ligands that is chemically adsorbed on the titania surface, creating the photoelectrode) and the redox active electrolyte (usually containing the I^-/I_3^- couple dissolved in an organic solvent). The circuit is closed with the use of a counter electrode (a thin layer of platinum or carbon on conductive glass) [2–4].

Without neglecting the role of the other components, the most crucial feature for efficient cell operation remains the optimization of the photoelectrode where light absorption along with electron collection are both realized. In this context, the semiconductor acts as a support for dye adsorption and as a sink for the injected electrons that are diffused following a random walk in the porous oxide network before being collected at the back contact [5,6]. Many factors can influence the effectiveness of the semiconductor, such as film morphology, structure, porosity, surface area, crystallinity, etc. [7,8]. In any event, a first prerequisite for TiO_2 is a large active surface area in order to adsorb the highest number of dye molecules and therefore achieve the maximum light harvesting. However, a large surface area can also introduce extra dislocations, impurities and defects, affecting directly the intrinsic properties of the material and consequently playing a critical role on the electron transport and recombination of the charge carriers, thus influencing both photocurrent and photovoltage of the cell.

In order to increase the TiO_2 surface area we can decrease, for instance, the particle size. However, it was found that when decreasing the particle size, the electron diffusion coefficients D_e are increased, while the recombination times (τ_e) are diminished [9]. In a similar paper, Chou et al. concluded that the largest particle size led to the highest short-circuit current and efficiency for the corresponding DSC [10]. Another way to increase the dye loading is the crystallinity modification; it was found that anatase (1 0 1) and rutile (1 1 0) surface planes are the preferred crystal orientations that promote dye anchoring [11]. However, simultaneously, rutile-based films have shown slower electron diffusion than the

* Corresponding authors. Tel.: +30 210 6503644; fax: +30 210 6511766.
E-mail addresses: stergt@chem.demokritos.gr (T. Stergiopoulos), papi@chem.demokritos.gr (P. Falaras).

1010-6030/$ – see front matter © 2010 Elsevier B.V. All rights reserved.
doi:10.1016/j.jphotochem.2010.10.015

anatase-based analogues, which was assigned to the more loosely packed structure of the rutile films [12].

It is then admitted that increasing surface area and dye loading are among the main requirements for an efficient cell since they improve light harvesting but, at the same time, affect, in a variant way (positive or negative), the electron dynamics in the semiconductor. Into this context, in this work, to study the aforementioned parallel effects, we chose to vary only the crystallinity and the aggregation/sintering degree of the semiconductor particles [13] by simply playing with the annealing conditions of titania (by varying the final temperature between 400 and 550 °C) that consisted of a powder (Degussa P25) with well defined morphology (spherical nanoparticles). In this way, the surface area and dye loading were altered, while TiO_2 particle shape variations with thermal annealing, i.e. particles creating tubes or rods, etc., was avoided, meaning that no extra implications arising from morphology modifications would have been taken place like in previous reports [14–16]. Moreover, no significant alterations were expected concerning the particle primary size, since this is controlled by the existing particles in nanostructured form of the precursor material. As expected, the obtained results, investigating in detail the structural properties along with the electron dynamics in the assembled DSCs, reveal a close interplay between the film nanostructure and light harvesting efficiency, electron transport, recombination and trapping, paving ways of how to proceed to the proper optimization of the photoelectrode's properties by increasing dye loading and simultaneously controlling electron dynamics.

2. Experimental

2.1. Preparation of TiO_2 paste, deposition on conductive glass and thermal treatment

The TiO_2 paste was prepared using Degussa P25 powder as starting material, following a well-known procedure [3]. In brief, 3 g of the powder were mixed with a 10% aqueous solution of distilled acetylacetone in a porcelain mortar, where deionized water was added dropwise. Finally, the mixture was further homogenized with a non-ionic surfactant, Triton X-100. The paste was then deposited on a pre-cleaned TEC15 transparent conductive glass substrate (Pilkington) using a glass rod [17]. The films were pre-heated at 120 °C for 30 min (heating rate of 5 °C min^{-1}) and subsequently fired at different final temperatures for 60 min. The annealing temperatures were 400, 450, 500 and 550 °C, respectively.

2.2. Characterization of TiO_2 films, sensitization and adsorption–desorption measurements

Crystallinity and crystalline size were determined from X-ray powder diffraction (XRD) using Cu K*a* radiation ($\lambda = 1.5418$ Å) on a Siemens D-500 spectrometer. Surface characterisation was undertaken using a JEOL JSM-5600 scanning electron microscope (SEM) with numerical image acquisition and a Digital Instruments Nanoscope III atomic force microscope (AFM) operating in the tapping mode [18]. The specific BET area of the films was estimated by nitrogen adsorption–desorption isotherms using a Sorptomatic 1990 Fisons Instrument. For photosensitization studies, the annealed TiO_2 films were immersed in 0.3 mM ethanolic solution of the N719 dye (Dyesol Ltd.) [19]. To determine the amount of the chemisorbed dye, adsorption–desorption experiments were performed on the TiO_2 films following a standard procedure [8]. UV–vis diffuse reflectance spectra of the dye sensitized TiO_2 films were obtained on a Hitachi 3010 spectrophotometer equipped with a 60 mm diameter integrating sphere.

2.3. Cell assembly, electrical and photovoltaic characterization

Non-sealed DSCs were fabricated by placing a drop of an ionic salt (PMII)-based liquid electrolyte (Dyesol Ltd.) onto the photoelectrode and sandwiching the counter electrode (CE) on top of the first electrode. The CE was a TEC15 glass onto which a very thin platinum layer was sputtered. The two electrodes were brought in close proximity with the help of an adhesive tape mask of about 50 μm, necessary to avoid short-circuiting between the two conductive glass surfaces. Current–voltage (*I–V*) measurements were performed by illuminating the DSCs using solar simulated light (1 sun, 1000 W m^{-2}) from a 300-W Xe source in combination with AM 1.5 and UV optical filters (Oriel). The *I–V* characteristics (under white light illumination and under dark) were obtained using linear sweep voltammetry on an Autolab PGSTAT-30 potentiostat (Ecochemie) working in a 2-electrode mode at a scan rate of 50 mV s^{-1}. Transport and recombination time constants were determined by intensity-modulated photocurrent spectroscopy (IMPS) and intensity-modulated voltage spectroscopy (IMVS), respectively, using the same system (Autolab) equipped with a frequency response analyzer (FRA). A red light (625 nm) emitting diode was used as the light source for both AC and DC illumination controlled by the FRA module. The dark charge extraction technique was also used (with the Autolab PGSTAT-30 potentiostat) according to the procedure developed in the literature in order to estimate the trapped charge at open-circuit [20].

3. Results and discussion

3.1. Morphological, structural and sensitization properties of the annealed TiO_2 films

Preliminary studies performed at 550 °C revealed little effect of the annealing time on the degree of the sintering and crystallinity of the particles. More precisely, the film thickness slightly decreases (from 12 μm to about 10.5 μm, Table S1) and stabilizes after 5 h of treatment. However, besides this, the XRD analysis and corresponding calculations using the Scherrer formula did not give evidence about any modification of the crystallite size (Fig. S1) and more importantly, the efficiency of the corresponding DSCs remains practically unaffected (Fig. S2 and corresponding values found at Table S1). Thus the final treatment temperature was limited at 60 min (1 h).

The lowest limit of the annealing temperature was set at 400 °C, since thermal analysis results (Fig. S3) have shown that almost complete decomposition of organic compounds (additives, residues) takes place at this temperature, thus facilitating the interconnection of titanium dioxide nanoparticles [21]. On the other hand, the annealing temperature was limited up to 550 °C as usual in related literature [9], since further increase may lead to degradation of the conductive glass. No significant variations were observed concerning the film thickness, which was found to be about 15.5 ± 1.5 μm (measured by a profilometer) for all the samples.

The crystallinity of the prepared films was investigated by XRD. The XRD patterns of films annealed at different temperatures in the range of 400 up to 550 °C are shown in Fig. S4. All diffraction patterns indicate a well-organized crystalline structure of titania NPs at all temperatures, revealing the characteristic peaks of the anatase and rutile phases of TiO_2 [17]. Crystallite sizes were estimated from the full width at half maximum of the main anatase diffraction peak at $2\theta \approx 25.2°$, using Scherrer's equation ($d = 0.9\lambda/B\cos\vartheta$) [22]. The anatase to rutile weight ratio x of the films was calculated from equation $x = (1 + 0.8I_A/I_R)^{-1}$ [23], where I_A and I_R correspond to the intensity of the anatase (1 0 1) and rutile (1 1 0) diffraction peaks at 25.2° and 27.4°, respectively. The obtained results, summarized

Table 1
Crystalline sizes and anatase/rutile percentages of the TiO_2 films annealed at different final temperatures (derived from XRD results).

Temperatures (°C)	Crystalline size (nm)	% Anatase	% Rutile
400	22.8	76.9	23.1
450	22.6	76.8	23.2
500	22.9	75.8	24.2
550	22.9	74.2	25.8

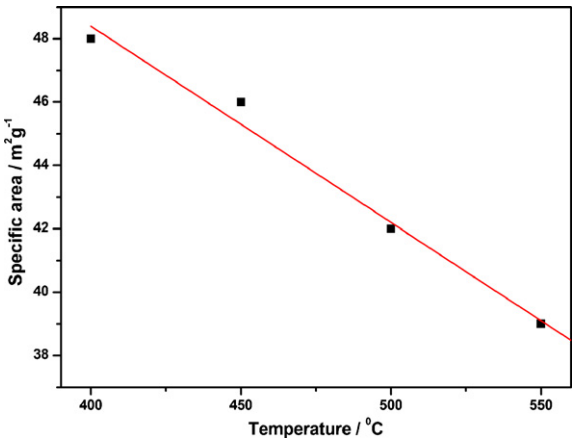

Fig. 1. Specific area (BET) values of the films derived from porosimetry measurements as a function of the final temperature.

in Table 1, confirm that the crystalline size does not vary appreciably for the temperature range studied here. This is expected since the mean diameter of nanocrystallites is controlled by the original semiconductor material (Degussa P25); modification with an organic carrier and subsequent thermal annealing does not induce an additional growth of the TiO_2 NPs. However, concerning the crystallinity of the samples (or the anatase/rutile weight ratio) as well as, there is a slight increase of the rutile amount at 550 °C from 23 up to about 26%.

Furthermore, SEM and AFM microscopies applied on the samples did not reveal any significant differences concerning the surface morphology of the nanocrystalline TiO_2 films. Representative top-view images are shown in Fig. S5 (for films annealed only at 550 °C), depicting that the surface consists of spherical NPs, fused together to form an extended interconnected network or aggregates of small size, exhibiting a sponge like porous rough structure.

The titania films were further characterized through the evaluation of their porous structure with nitrogen adsorption–desorption isotherms by scratching the material off the glass substrate. The significant hysteresis loop observed in all isotherms confirms the mesoporous character of the Degussa P25 nanopowder [24], independent of the annealing procedure implying that the mesoporous structure is preferred independently to the high annealing temperature (representative adsorption–desorption isotherms are shown in Fig. S6 for films annealed at 550 °C). The specific surface area (BET) decreases linearly from 48 to 39 $m^2 g^{-1}$ (Fig. 1) with the increase of the calcination temperature, in agreement with literature [14]. These values were lower than those of the original Degussa P25 material (57 $m^2 g^{-1}$). Taking into account the fact that the particle size was not significantly affected, we can infer that the decrease of the BET area (about 19%) is mainly caused by the partial aggregation of the TiO_2 NPs (confirmed by the SEM and AFM analysis) and the neck growth of the particles, i.e. the small particles get merged or connected together due to the elevated temperature conditions [25].

All the above parameters (particle size, crystallinity and surface extension) affect the dye chemisorption and consequently the light harvesting of the sensitized films. In this context, it is very interesting to estimate directly the effectiveness of the titania photoelectrodes on the adsorption of the N719 dye. For this purpose, adsorption–desorption measurements of the sensitizer were performed. Subsequently, the roughness factors (RFs) of the films, representing their actual ability for dye loading, were determined. The calculated RFs (summarized in Table 2) follow the same trend as the one observed in the BET measurements; they decrease from 1010 down to 613 with increasing temperature from 400 to 550 °C, indicating that high calcination temperatures lead to lower dye uptake resulting from the reduction of BET area, in accordance with other previous results [16]. UV–vis diffuse reflectance spectra (Fig. S7) of the films confirm that light harvesting is consecutively reduced by increasing temperature, while absolute similarities in the absorbance of the films at long wavelengths (>600 nm) imply that no significant light scattering takes place probably due to the small size of aggregates, created during annealing.

3.2. Photovoltaic and photoelectrochemical properties of the annealed films incorporated in DSCs

In the previous section, we figured out that the BET surface area and dye loading determine the light harvesting of the photoelectrodes. However, we must notice that other considerable factors like transport and recombination inside the semiconductor can be also seriously affected. To investigate the above probability, the photovoltaic performance of the sensitized films was thoroughly examined after their incorporation in sandwich-type solar cells. The current–voltage characteristics of DSCs are depicted in Fig. 2a, while Table 2 summarizes the cell performance and the corresponding parameters derived from the *I–V* curves. The power conversion efficiency (η) attained, strongly depends on the calcination temperature, with the highest, 6.41%, obtained by DSCs based on titania films calcined at 550 °C. This specific trend was also observed for the short-circuit photocurrent (J_{sc}). On the contrary, the other electrical parameters derived from the *I–V* characteristics presented a different behaviour.

More specifically, the values of the open-circuit potential (V_{oc}) show a sharp increase from 740 to 783 mV between 400 and 450 °C, while further temperature increase from 450 to 550 °C, leads to slightly higher values of V_{oc} stabilized at about 790 mV (within experimental error). The V_{oc} magnitude is mainly affected by the recombination of conduction band electrons with I_3^- ions (and with dye cations to a lesser extent), taking place near open-circuit conditions. To investigate the back reaction with the electrolyte, *I–V* curves under dark were measured (Fig. 2b). For all cells, the onset of cathodic current was observed beyond −500 mV vs. Pt. As the cal-

Table 2
Performance of solar cells as a function of the calcination temperature. The roughness factors of the films determined through adsorption–desorption measurements are also presented.

Temperature (°C)	V_{oc} (mV)	J_{sc} (mA cm^{-2})	FF	η (%)	Roughness factor
400	740	11.09	0.65	5.31	1010
450	783	11.67	0.59	5.40	851
500	784	12.51	0.57	5.58	703
550	786	13.33	0.61	6.41	613

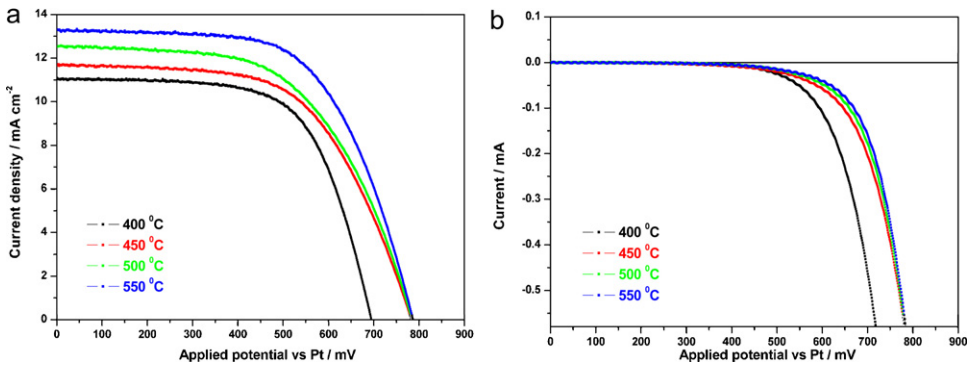

Fig. 2. Current–voltage (*I–V*) characteristics of the DSCs based on film electrodes calcined at different final temperatures obtained under 1 sun (AM 1.5) illumination (a) and under dark (b), respectively.

cination temperature increases from 400 to 450 °C, there is a 60 mV displacement of the curve, while for all the other cells (450–550 °C), the *I–V* curves practically coincide, in perfect agreement with the obtained V_{oc} values (Table 2).

To get more insight into the origin of the above behaviour, IMVS was initially used. Fig. 3 presents the plot of the electron lifetime τ_n (under open-circuit conditions) versus incident light intensity. For all cells, τ_n exhibits an exponential dependence on the light intensity, which can be explained by the exponential distribution of traps inside TiO_2 band gap [26]. The values of the electron lifetime range from 5 to 8 ms at high bias light intensities (800 W m^{-2} or 2.5×10^{17} photons cm^{-2} s^{-1}), while they increase up to 25–63 ms for lower light illumination. Under high illumination intensities that approach quite well the 1 sun (i.e. steady-state) conditions, the electron lifetimes at 400 °C are shorter (5 ms) than in other temperatures, implying that the lower V_{oc} can be partly attributed to the lower τ_n. On the other hand, the electron lifetime was practically constant (about 8 ms) in the temperature range of 450–550 °C, in qualitative agreement with the measured V_{oc} values [27].

In order to obtain information about the trap density in the semiconductor, the electronic charge at open-circuit was measured by performing charge extraction experiments in the dark. Fig. 4 presents the extracted electron density (n_{ext}) versus the applied cell voltage (V_{cell}, which equals the difference between E_F and E_{redox}, E_F being the Fermi level energy and E_{redox} the Nernst potential of the redox couple). At 400 °C, the stored charge is significantly higher (attaining values of 4×10^{18} cm^{-3}) compared to that obtained at higher temperatures. The high electron density at high V_{cell} (or at E_F values approaching E_c) confirms the presence of a large amount of shallow traps that accelerate recombination kinetics [28], in excellent agreement with lower electron lifetime and V_{oc} produced by the cell. These traps might derive from defects due to oxygen deficiency directly related to the larger BET surface area [29] of the films annealed at 400 °C; oxygen vacancies have been shown to act as shallow traps in titanium dioxide [30]. At all the other temperatures studied, no significant differences are observed in the range of V_{cell} values approaching V_{oc}, implying that the density of shallow trap states does not practically change with the annealing temperature, thus not affecting recombination dynamics (in perfect agreement with the IMVS results). It appears that annealing at 450 °C is capable of filling up oxygen vacancies in TiO_2 [31], whereas further annealing up to 550 °C does not influence this process.

Despite the fact that the V_{oc} values were only slightly influenced by the annealing process (while the FF was practically unaffected), the most significant feature of the *I–V* curves is the increase of J_{sc} from 400 to 550 °C (from 11 up to 13 mA cm^{-1}) despite the reduced dye loading and consequently diminished light harvesting. This implies that the current is increased due to improved injection and/or collection efficiency. Even though charge injection efficiencies could not be directly measured here [32], previous studies confirmed that injection dynamics are slightly affected by the annealing temperature of the TiO_2 film [33]. Despite the fact that this probability cannot be excluded, the charge collection seems to be mostly affected by the annealing temperature. At this point, it should be noted that the transmittance (*T*) of the conductive glass annealed (alone) is identical for all temperatures ($T = 82 \pm 1\%$ at the 400–700 nm wavelength region), implying that no changes

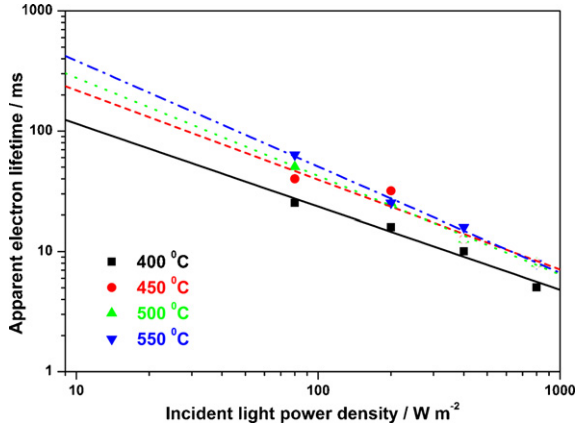

Fig. 3. Electron lifetime versus the incident power density derived from IMVS experiments on DSCs based on films calcined at different final temperatures.

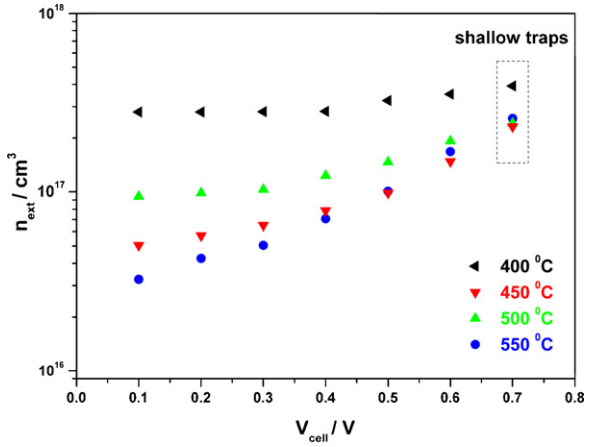

Fig. 4. Semi-logarithmic plot of the extracted electron density vs. cell potential measured under controlled voltage conditions in the dark for DSCs using TiO_2 anodes annealed at different temperatures. Note that $V_{cell} = E_F - E_{Redox}$ (in the border in dash lines, the region of potentials that correspond to shallow states are shown – see details in the text).

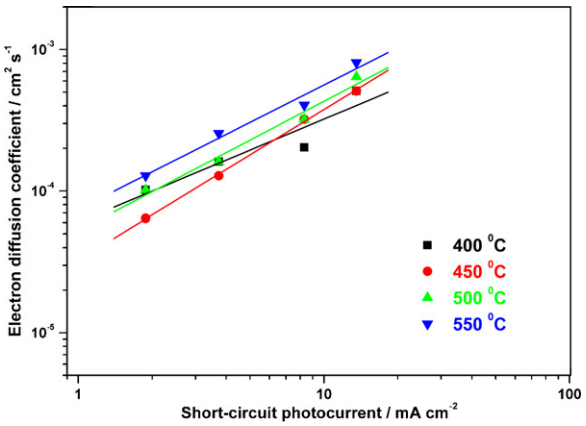

Fig. 5. Electron diffusion coefficients (D_e) calculated from IMPS versus the DC photocurrent delivered by the DSCs prepared by films annealed at different temperatures.

on the light reaching the sensitized titania film were induced by the thermal treatment of the conductive glass at high temperatures (affecting the delivered photocurrent). Likewise, 4 point resistance results on the above samples verified that no change in the bulk resistivity of the conductive glass occurred during annealing (Fig. S8).

In order to study electron transport, IMPS was subsequently used to estimate the electron diffusion coefficients (D_e) at different J_{sc} values (Fig. 5). The diffusion coefficients were in the range of 1 to 9×10^{-4} cm^2 s^{-1}, in agreement with literature results [34]. The D_e follows exactly the same trend as the measured J_{sc} values; they increase with the increase of the annealing temperature [35]. In this temperature range, the BET area is progressively reduced, the rutile content is increased (that would normally decrease D_e [34]) and the TiO_2 particle size remains constant, implying that the D_e increase is due to the neck growth of the particles [16], postulating that the concomitant increase of the number of interconnects between TiO_2 nanoparticles decreases the resistance for electrons for electrons to hop from one particle to another.

4. Conclusions

Following a careful investigation of the intrinsic properties of the semiconductor, their influence on internal resistances, electron transport, recombination and trapping at surface states was confirmed. In addition, their correlation with the structural modifications and photoelectric conversion efficiency of the corresponding dye-sensitized solar cells (DSCs) was established.

In fact, efficient control of the semiconductor properties, maximum dye loading and simultaneous optimization of electron dynamics were revealed as the main parameters determining the performance of a DSC. Investigating the interdependence of these processes, in this work, we have confirmed that the final annealing temperature of TiO_2 photoelectrodes mainly affects the crystallinity, sintering and aggregation of the nanoparticles. In addition, the connection between the structure of the semiconductor with its electrical properties and finally its photoelectrochemical behaviour as anode in a DSC was established.

The obtained results allowed us to identify distinct temperature regimes: At 400 °C, the efficiency is as high as 5.3% accompanied with the higher dye loading. The presence of a large amount of surface states, due to the higher BET surface area, leads to shorter electron lifetimes and V_{oc}, while the lower values of diffusion coefficients and J_{sc} postulate the presence of insufficient neck growth. In the range of 450–550 °C, the films generally exhibit similar morphological and crystalline properties, while the increase of annealing temperature results in higher efficiencies reaching 6.4% at 550 °C, despite the lower light harvesting induced by a relative decrease in the surface area. This behaviour arises from the enhancement of the electron diffusion coefficient D_e, assigned to the improved neck growth (interconnectivity) between particles.

Acknowledgements

The work is dedicated to Prof. N. Spyrellis. The authors acknowledge financial support from the General Secretariat for Research and Development (GSRT – Greece) through 03ED 118/2005 "PENED" project. T. S. thanks the Greek State Scholarships Foundation (IKY) for fellowship allowance. Helpful assistance from Dr. V. Psyharis (XRD analysis), Dr. V. Likodimos (Raman spectra), D.S. Tsoukleris (AFM images), Dr. A.G. Kontos (UV–vis measurements) Dr. K. Papadokostaki (TGA analysis) and Dr. P. Dimitrakis (resistivity measurements) is also acknowledged.

Appendix A. Supplementary data

Supplementary data associated with this article can be found, in the online version, at doi:10.1016/j.jphotochem.2010.10.015.

References

[1] B. O'Regan, M. Grätzel, A low-cost, high efficiency solar-cell based on dye-sensitized colloidal TiO_2 films, Nature 353 (1991) 737–740.
[2] A Hagfeldt, M. Grätzel, Light-induced redox reactions in nanocrystalline systems, Chem. Rev. 95 (1995) 49–68.
[3] M.K. Nazeeruddin, A. Kay, I. Rodicio, R. Humphry-Baker, E. Muller, P. Liska, N. Vlachopoulos, M. Grätzel, Conversion of light to electricity by cis-X_2bis(2,2′-bipyridyl-4,4′-dicarboxylate)ruthenium charge-transfer sensitizers (X = Cl^-, Br^-, I^-, CN^-, and SCN^-) on nanocrystalline TiO_2 electrodes, J. Am. Chem. Soc. 115 (1993) 6382–6390.
[4] R. Sivakumar, A.T.M. Marcelis, S. Anandan, J. Photochem, Synthesis and characterization of novel heteroleptic ruthenium sensitizer for nanocrystalline dye-sensitized solar cells, Photobiol. A: Chem. 208 (2009) 154–158.
[5] N. Kopidakis, E.A. Schiff, N.–G. Park, J. van de Lagemaat, A.J. Frank, Ambipolar diffusion of photocarriers in electrolyte-filled, nanoporous TiO_2, J. Phys. Chem. B 104 (2000) 3930–3936.
[6] A.C. Fisher, L.M. Peter, E.A. Ponomarev, A.B. Walker, K.G.U. Wijayantha, Intensity dependence of the back reaction and transport of electrons in dye-sensitized nanocrystalline TiO_2 solar cells, J. Phys. Chem. 104 (2000) 949–958.
[7] N.G. Park, K. Kim, Transparent solar cells based on dye-sensitized nanocrystalline semiconductors, Phys. Stat. Sol. (a) 205 (2008) 1895–1904.
[8] T. Stergiopoulos, A. Ghicov, V. Likodimos, D.S. Tsoukleris, J. Kunze, P. Schmuki, P. Falaras, Dye-sensitized solar cells based on thick highly ordered TiO_2 nanotubes produced by controlled anodic oxidation in non-aqueous electrolytic media, Nanotechnology 23 (2008) 235602.
[9] S. Nakade, Y. Saito, W. Kubo, T. Kitamura, Y. Wada, S. Yanagida, Influence of TiO_2 nanoparticle size on electron diffusion and recombination in dye-sensitized TiO_2 solar cells, J. Phys. Chem. B 107 (2003) 8607–8611.
[10] T.P. Chou, Q. Zhang, B. Russo, G.E. Fryxell, G. Cao, Titania particle size on the overall performance of dye-sensitized solar cells, J. Phys. Chem. C 111 (2007) 6296–6302.
[11] Y. Lu, D.-J. Choi, J. Nelson, O.-B. Yang, B.A. Parkinson, Adsorption, desorption, and sensitization of low-index anatase and rutile surfaces by the ruthenium complex dye N3, J. Electrochem. Soc. 153 (2006) E131–E137.
[12] N.G. Park, J. van de Lagemaat, A.J. Frank, Comparison of dye-sensitized rutile- and anatase-based TiO_2 solar cells, J. Phys. Chem. B 104 (2000) 8989–8994.
[13] R.S. Rawat, V. Aggarwal, M. Hassan, P. Lee, S.V. Springham, T.L. Tan, S. Lee, Nano-phase titanium dioxide thin film deposited by repetitive plasma focus: Ion irradiation and annealing based phase transformation and agglomeration, Appl. Surf. Sci. 255 (2008) 2932–2941.
[14] K. Wessels, M. Minnermann, J. Rathousky, M. Wark, T. Oekermann, Influence of calcination temperature on the photoelectrochemical and photocatalytic properties of porous TiO_2 films electrodeposited from Ti(IV)-alkoxide solution, J. Phys. Chem. C 112 (2008) 15122–15128.
[15] J. Qu, X.P. Gao, G.R. Li, Q.W. Jiamg, T.Y. Yan, Structure transformation and photoelectrochemical properties of TiO_2 nanomaterials calcined from titanate nanotubes, J. Phys. Chem. C 113 (2009) 3359–3363.
[16] D. Zhao, T. Peng, L. Lu, P. Cai, P. Jiang, Z. Bian, Effect of annealing temperature on the photoelectrochemical properties of dye-sensitized solar cells made with mesoporous TiO_2 nanoparticles, J. Phys. Chem. C 112 (2008) 8486–8494.
[17] I.M. Arabatzis, S. Antonaraki, T. Stergiopoulos, A. Hiskia, E. Papakonstantinou, P. Falaras, Preparation, characterization and photocatalytic activity of

nanocrystalline thin film TiO_2 catalysts towards 3,5-dichlorophenol degradation, J, Photochem. Photobiol. A: Chem. 149 (2002) 237–245.
[18] D.S. Tsoukleris, I.M. Arabatzis, E. Chatzivasiloglou, A.I. Kontos, V. Belessi, M.C. Bernard, P. Falaras, 2-Ethyl-1-hexanol based screen-printed titania thin films for dye-sensitized solar cells, J. Solar Energy 9 (2005) 422–430.
[19] M.K. Nazeeruddin, R. Humphry-Baker, P. Liska, M. Grätzel, Investigation of sensitizer adsorption and the influence of protons on current and voltage of a dye-sensitized nanocrystalline TiO_2 solar cell, J. Phys. Chem. B 107 (2003) 8981–8987.
[20] J.R. Jennings, A. Ghicov, L.M. Peter, P. Schmuki, A.B. Walker, Dye-sensitized solar cells based on oriented TiO_2 nanotube arrays: Transport, trapping, and transfer of electrons, J. Am. Chem. Soc. 130 (2008) 13364–13372.
[21] H. Hoshikawa, M. Yamada, R. Kikuchi, K. Eguchi, Impedance analysis of internal resistance affecting the photoelectrochemical performance of dye-sensitized solar cells, J. Electrochem. Soc. 152 (2005) 68–73.
[22] H.P. Klug, L.E. Alexander, X-Ray Diffractions procedures, 9, Wiley, New York, 1954, p.491.
[23] B.D. Cullity, S.R. Stock, Elements of X-ray Diffraction, third ed., Prentice Hall Inc., Upper Saddle River, NJ, 2001.
[24] Y. Chen, E. Stathatos, D.D. Dionysiou, Microstructure characterization and photocatalytic activity of mesoporous TiO_2 films with ultrafine anatase nanocrystallites, Surf. Coat. Technol. 202 (2008) 1944–1950.
[25] S. Nakade, M. Matsuda, S. Kambe, Y. Saito, T. Kitamura, T. Sakata, Y. Wada, H. Mori, S. Yanagida, Dependence of TiO_2 nanoparticle preparation methods and annealing temperature on the efficiency of dye-sensitized solar cells, J. Phys. Chem. B 106 (2002) 10004–10010.
[26] A.V. Barzykin, M. Tachiya, Mechanism of charge recombination in dye-sensitized nanocrystalline semiconductors: Random flight model, J. Phys. Chem. B 106 (2002) 4356–4363.
[27] W.H. Howie, F. Claeyssens, H. Miura, L.M. Peter, Characterization of solid-state dye-sensitized solar cells utilizing high absorption coefficient metal-free organic dyes, J. Am. Chem. Soc. 130 (2008) 1367–1375.
[28] J. Bisquert, A. Zaban, M. Greenshtein, I. Mora-Seró, Determination of rate constants for charge transfer and the distribution of semiconductor and electrolyte electronic energy levels in dye-sensitized solar cells by open-circuit photovoltage decay method, J. Am. Chem. Soc. 126 (2004) 13550–13559.
[29] M.K. Nowotny, L.R. Sheppard, T. Bak, J. Nowotny, Defect chemistry of titanium dioxide. Application of defect engineering in processing of TiO_2-based photocatalysts, J. Phys. Chem. C 112 (2008) 5275–5300.
[30] S. Duenas, H. Garcia, E. San Andres, M. Toledano-Luque, I. Martil, G. Gonzalez-Diaz, K. Kukli, T. Uustare, J. Aarik, A comparative study of the electrical properties of TiO_2 films grown by high-pressure reactive sputtering and atomic layer deposition, Semicond. Sci. Technol. 20 (2005) 1044–1051.
[31] J. Bisquert, Theory of the impedance of electron diffusion and recombination in a thin layer, J. Phys. Chem. B 106 (2002) 325–333.
[32] J. Kallioinen, G. Benko, P. Myllyperkio, L. Khriachtchev, B. Skårman, R. Wallenberg, M. Tuomikoski, J. Korppi-Tommola, V. Sundstrom, A.P. Yartsev, Photoinduced ultrafast dynamics of $Ru(dcbpy)_2(NCS)_2$-sensitized nanocrystalline TiO_2 films: The influence of sample preparation and experimental conditions, J. Phys. Chem. B 108 (2004) 6365–6373.
[33] L.M. Peter, Dye-sensitized nanocrystalline solar cells, Phys. Chem. Chem. Phys. 9 (2007) 2630–2642.
[34] K. Zhu, N. Kopidakis, N.R. Neale, J. van de Lagemaat, A.J. Frank, Influence of surface area on charge transport and recombination in dye-sensitized TiO_2 solar cells, J. Phys. Chem. C 110 (2006) 25174–25180.
[35] P.R.F. Barnes, A.Y. Anderson, S.E. Koops, J.R. Durrant, B.C. O' Regan, Electron injection efficiency and diffusion length in dye-sensitised solar cells derived from incident photon conversion efficiency measurements, J. Phys. Chem. C 113 (2009) 1126–1136.